Characterization of an electrostatic filter prototype for bioaerosol flowmetering for INTA Investigation Aerial Platforms

Suthyvann Sor[1], Rafael Bardera[1], Adelaida Garcia-Magariño*[1]
Elena Gonzalez[2], Mª Ángeles Aguilera[2],
[1]Instituto Nacional de Tecnología Aeroespacial, Torrejón de Ardoz, Spain
[2]Centro de Astrobiología, CAB-INTA-CSIC, Torrejón de Ardoz, Spain

*Corresponding author: garciamga@inta.es

Abstract
The characterization of the airborne microorganisms at different altitudes of the atmosphere is usually conducted by means of aerial platforms. It is very interesting to know the biological processes in the atmosphere. However, there are problems associated to the fact that sampling systems are embarked on an aircraft and the low presence of microorganisms at high altitude. A prototype of a new electrostatic filter for bioaersol flowmetering dedicated to biology investigations has been developed. This prototype was designed to be installed on board aerial platforms of INTA. The experimental characterization of the aerodynamic flow was performed in order to investigate the behaviour of the filter when different air intake widths and different mechanical deflectors are employed. A combination of these impactor with the filters based on industrial electrostatic precipitator technology have been studied. Non-intrusive Particle Image Velocimetry technique has been used to measure the flow field inside the filter when it was running under controlled conditions in laboratory. This study is a first investigation on the flow field of filter for bioaerosol flowmetering to be embarked on an aircraft. The results show the influence of each parameter in the flow field that could be used for further investigations and designs.

Keywords
Aerial platforms, Bioaerosol, Electrostatic filter, Impactor filter.

1. Introduction

The aim of the project “Scientific missions from manned and unmanned aerial platforms” is the study of microorganisms present in the atmosphere by collecting bioaerosols from INTA’s Investigation Aerial Platforms.
A qualitative and quantitative characterization of the airborne microorganisms at different altitudes of the atmosphere is very interesting to know the biological processes in the atmosphere. Bioaerosols are formed by particles of biological origin that are present in all environments, including viruses, bacteria, proteins, fungal spores, pollens and other components, residues or products of organisms. Particle size for bioaerosol ranges are typically from less than 1 µm up to 100 µm [1]. This study is steered to filtering mainly bacteria and viruses. Bacteria are single-cell microorganisms that range in physical size from 0.5 to 30 µm [2]. The aerodynamic size of most of bacteria in relatively clean environments has been reported to be 1 to 3 µm [2]. On the other hand, viruses are intracellular parasites because they can reproduce only inside a host cell. Some studies performed by Blechere et al [3] determined that 50% of total viral particles analysed were in the range < 4 µm and about 5% in the range < 1 µm.

Several types of filters were developed to research or industrial applications [1, 2]. Based on inertial impaction some specifically designed to bioaerosols filtering were found as the Andersen cascade impactor [4, 5], biosampler Swirling Aerosol Collector (SKC impinger) (1) or All Glass Impinger (AGI 30) [1, 2]. Also, electrostatic filtering based on industrial electrostatic precipitator technology was applied to bioaerosol sampling [6, 7]. The most recent bioaerols samples reviews are those of Ghosh et al in 2015 [8] and Haig et al in 2016 [9], which are focused on bioaerols samples indoor. Literature concerning this kind of filters reports high effectivity collecting samples when they are working in laboratory condition at very low mass flow rate. However, collecting efficiencies decrease when the flow rate is increased, the collecting time is reduced or the wind inlet velocity is increased [8], as happens when they are installed on board the aircraft. The authors have not found literature regarding bioaerosol sampling method designed to be embarked in an aircraft. Therefore, the application of traditional sampling method to be embarked in aircrafts is an open field. The particularities of the sampling system to collect bioaerosols in the atmosphere during flight tests are discussed in more detail in the next section.

An isokinetic sampling system was designed to be embarked on INTA's Investigation Aerial Platforms because this kind of sampling has been recognized as the only way to obtain an accurate and representative sample of particles present in the atmosphere [10, 11]. The isokinetic intake allows to know the concentration of particles present in the atmosphere, since the flow streamlines are parallel at the inlet and the total amount of particles would follow the flow and enter into the sampling system. This sampling system mainly consists of an isokinetic intake probe and a filtering system dedicated to separate the bioaerosol particles during tests flight campaign to be analysed later in ground laboratory by microscopy techniques. Figure 1 shows a sketch of the system embarked in the aircraft C212, which is the main INTA Investigation Aerial Platforms. A pump (shown in marron in Fig. 1) is necessary to be able to adjust the intake velocity to obtain an isokinetic intake.

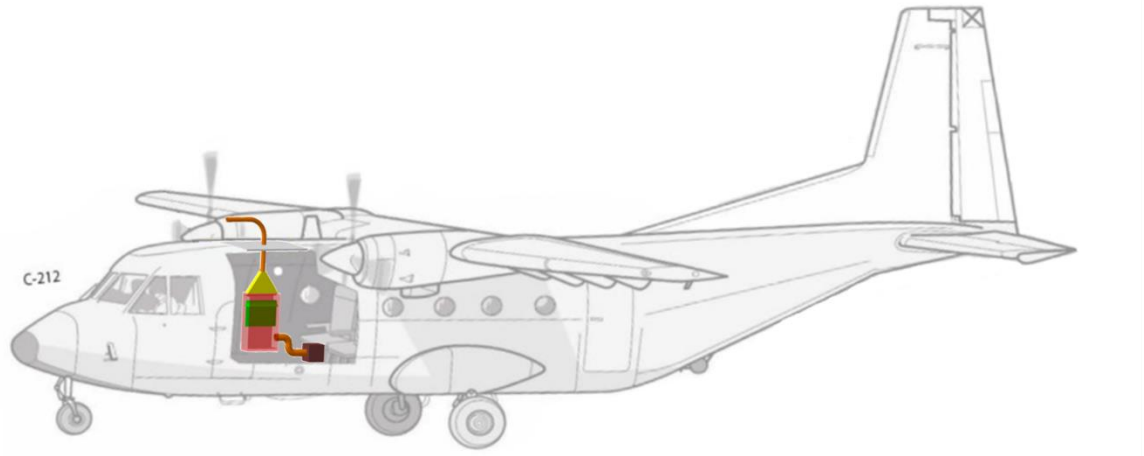


Figure 1. Sketch of the system embarked in the aircraft C212.

A dry type of impactor filter was selected as most adequate to be embarked on the INTA's aircraft during the microorganisms collection in flight due to the possible vibration during the take-off and landing. Taking into account the usual cruising speed of the aircraft is 100 m/s (360 km/h) an expander cone was installed in the sampling pipe to reduce the velocity at the filter inlet to be of order of 20 m/s (see Fig. 2). Following this philosophy, some prototypes of filters have been designed, built and tested with different configurations in order to characterize the internal flow inside the filter. Both numerical simulations and experimental non-intrusive technique Particle Image Velocimetry (PIV) have been used to measure the flow field velocity inside the filter. A comparative analysis of results was performed in order to obtain the optimized filter to be aircraft-mounted for collection of microorganisms from the upper atmosphere. Finally, tests to obtain the magnitude order of the efficiency were performed.

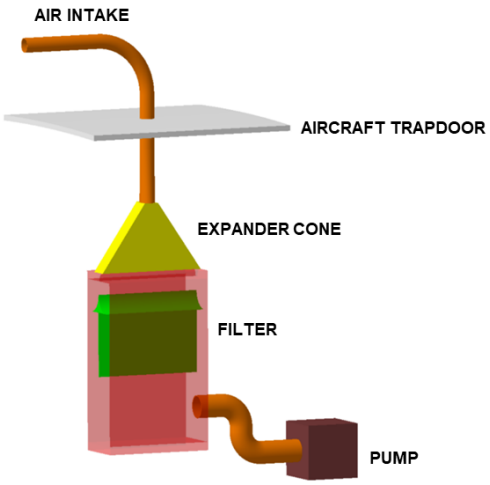


Figure 2. Sketch of the sampling system.

2. Particularities of the samples systems to collect bio-aerosols in the atmosphere during flight tests.

Though sampling system to collect particles indoor could be applied to collect particles in-flight, the efficiencies would decrease considerable (as discussed in the introduction), and therefore new designs or improvements in the existing design should be conducted. The main differences that appear in the design process as a consequence of the fact of being used in-flight follows:

- ***Flow Rate.*** In the atmosphere, the bio-aerosols concentration is considerable lower than indoors, and therefore the flow rate used to collect the particles should be greater so as to collect similar amount of aerosols.

- ***Collecting Time.*** The collecting time is a limitation factor since a minimum number of particles of bioaerosols should be collected to be able to analyse the data obtained. The aircraft passes through a specific area of the atmosphere, where the collection is conducted, and the collecting time is only the time during the pass, which depend on the aircraft velocity and the extension of the specific area. The cruise velocity of the aircraft is usually on the order of 100 m/s. The collecting time is usually less than half an hour.

- ***Inlet Conditions.*** Finally, the last difference respect to the sampling method design to collect particles indoors is the inlet conditions, on the order of 20 m/s. Generally, higher inlet wind speed lead to lower collecting efficiencies. Reduced collecting efficiency has been found to be correlated with increasing flow rate for indoor sampling systems. The collection efficiency can be reduced from 99% in still air to 9.6% with wind speed across the inlet of 4.5m/s [8].

Therefore, it is apparent the need of studying the flow inside the filters in order to gain insight into the problem and be able to design new filters with higher efficiencies for higher inlet wind velocities and higher flow rate.

3. Prototypes Description

The electrostatic filters built for this investigation are based on DC corona effect. Electrodes were fed by a high voltage generator TREK model 20/20 C connected to an Agilent 33500B functions generator. The type of electrostatic filter used in this investigation consists of two outer electrodes in the form of metallic plates and a central ionizing deflector electrode maintained to high electric potential (See Figure 3). The difference of potential between plates and central electrode creates an electric field. As electrodes are at high voltage, it is generated a corona effect that ionizes the surrounded atmosphere. The particles passing through the filter acquire electric charge and once charged are subjected to a transverse electrostatic force that pulls them towards the collecting plates. In the down side, a cylindrical tube that has a spline hole in the down side is connected to a vacuum pump that creates a suction to produce the motion of the air.

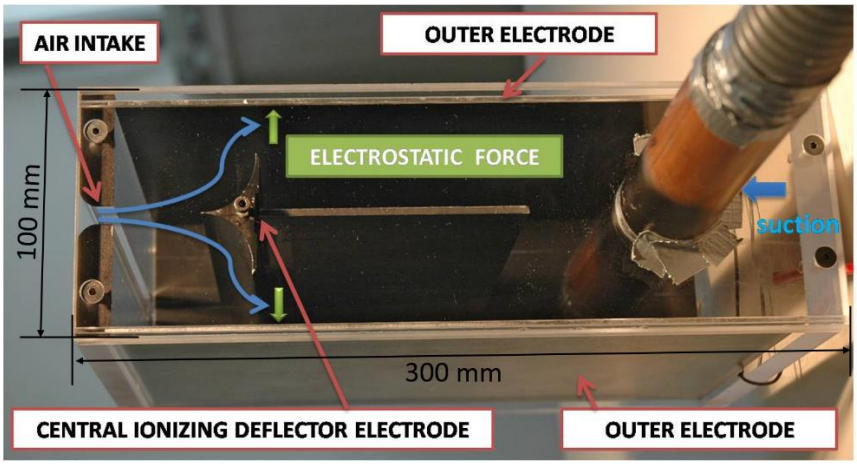


Figure 3. Electrostatic filter concept. The large blue lines represent the air flow direction while the green arrows represent the electrostatic forces. Dimensions of the filter are display in black.

FILTER #	INTAKE WIDTH d_i (mm)	DEFLECTOR WIDTH D (mm)	DEFLECTOR TYPE	INTAKE VELOCITY u (m/s)
1	35	55	flat plate	6
2	7	55	flat plate	27
3	7	55	flat plate	20
4	7	65	flat plate	20
5	7	55	curvature radius 24 mm	20

Table 1. Electrostatic filters design parameters.

Five different configurations were investigated, corresponding to different air intake width and different mechanical deflectors according to Table 1. The width of the filters was 100 mm and the total height was 300 mm. The filters span was 200 mm. The five filters used are shown in figures 4 and 5. Filters 1 and 2 can be observed in figure 1. The difference between them is the width of the air intake orifice, being 35 mm in the Filter 1 and 7 mm in the Filter 2. Both filters have the same mechanical deflector: a flat plane of 55 mm width. The vacuum pump employed was regulated at its maximum suction power (which correspond to an intake air velocity of approximately 9 m/s for Filter 1 and 27 m/s for Filter 2). Figure 3 shows the other filters (Filter 3, Filter 4 and Filter 5), where the difference between them was the mechanical deflector employed. A flat plate perpendicular to the mechanical deflector was added in the rear side of each deflector to increase the symmetry. This flat plate was in contact to the mechanical deflector, and consequently at the same voltage. The width of the mechanical deflector of the Filters 3 and 5 was 55 mm (see figure 5), while the width of the mechanical deflector of Filter 4 was 65 mm. The curvature radius of the mechanical deflector of Filter 5 was 24 mm. The air intake width was 7 mm, the same as in Filter 2, and the pump was also the same pump but working at its minimum suction power (which corresponds to an air intake velocity on the order of 20 m/s).

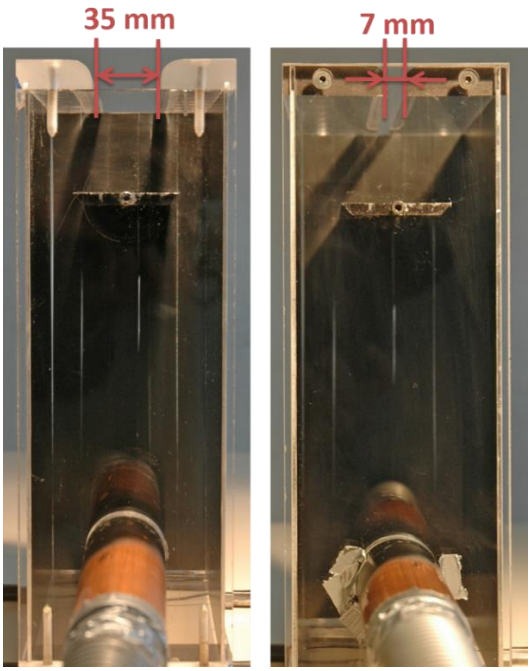


Figure 4. Photographs of Filter 1 (on the left) and Filter 2 (on the right). Dimensions of the mechanical deflectors displayed in red.

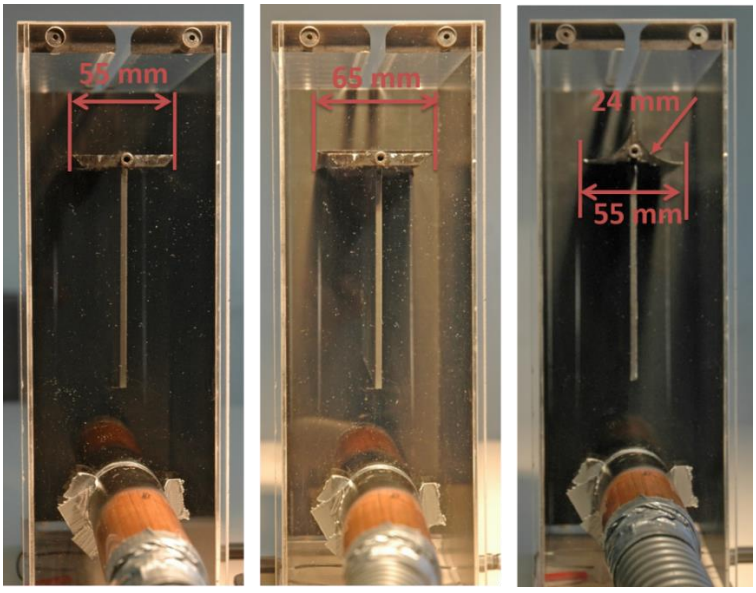


Figure 5. Photographs of Filter 3 (on the left), Filter 4 (in the centre) and Filter 5 (on the right). Dimensions of the mechanical deflectors displayed in red.

4. Experimental Setup

Experimental Setup

The flow field velocity for each filter was measured using the particle image velocimetry technique [12-13]. A picture of the experimental setup is shown in figure 6. A commercial PIV system from TSI Inc. was used. Flow illumination was provided by two pulsed Nd:YAG 190 mJ laser, whose pulse lasted for 8 ns. Images were taken using a Power View Plus 4MP camera with a resolution of 2048 x 2048 pixels. Data transmission was made directly to the PC RAM via a 64-bit camera link which allows for an information transfer up to 512 MB per second. The camera lens was AF Nikkor 80-200mm f/2.8 D. Olive oil droplets were used as seeding particles, which are known to be charged particles, having a diameter of one micron, which is the usual size in PIV experiments. Synchronization between image capturing and flow illumination and the analysis was carried out using the TSI Insight 3G software and a Laser Pulse synchronizer. The time Δt between two consecutive laser pulses was 25 μs. The flow field for the first two filters was 174 mm × 174 mm, while for the other three filters was 256 mm × 256 mm. The resolutions were 85 μm/pixel and 125 μm/pixel, respectively. Each PIV image was divided into smaller sub-interrogation areas containing 32 pixels × 32 pixels. Each recording sequence consisted of 100 pair of images. A post-processing was also employed to interpolate and replace spurious vectors. Then the average velocity map are calculated.

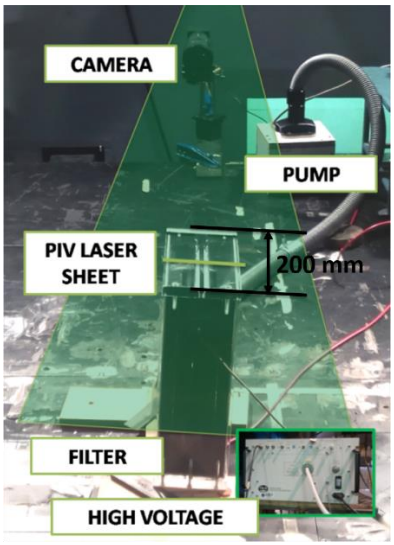


Figure 6. Photograph of the Experimental Experiment Setup. PIV laser sheet is superimposed in green. Dimensions are displayed in black.

Particle Image Velocimetry Validity Discussion

PIV system to measure flow velocity is based on the assumption that the seeding particles follow the flow. The Stokes number is a measure of flow tracer fidelity and it is defined as the ratio of the characteristic time of the particle to a characteristic time of the flow. The Reynolds number of the particles is on the order of the unity and assuming stokes flow, the characteristic time is calculated, being on the order of 3 ns. In general, the characteristic time of the flow could be calculated as the velocity of the flow divided to the particle diameter, which in this case leads to a value on the order of 20 μs. Therefore, the Stokes number would be much less than unity and the particles would follow the flow. However, when the flow decelerates abruptly, the characteristic time of the flow depends on the deceleration, which is unknown a priori. If the deceleration values are very high, then the characteristic time of the flow is very short, and it may happen that the seeding particles would not follow the flow. In that case, the air velocity measurement would not be valid, since the PIV measurement would provide air velocity, but instead only the seeding particle velocity. Fortunately, the real interest in studying the flow is to study the motion of biaerosols, whose diameters range from 1 to 100 μm. The seeding particles have a size on the order of 1 μm, which is the smallest diameter of bioaerosol that are addressed in this investigation. Therefore, when the deceleration reaches values that particles of 1 μm can no longer follow, the measurements obtained by PIV are the velocities of these particles, which provides valuable information in the investigation. To check that the particles indeed impact the impact zone, instead of the side plates walls, two walls made of methacrylate were used and a photograph was taken at the end. Figure 7 shows this photograph, showing how indeed the particles impact the impact zone in the walls. In the real situation embarked onboard, more particles above 1 μm would impact on the walls where particles of 1 μm do not impact, and it would depend on the deceleration values and the particles size.

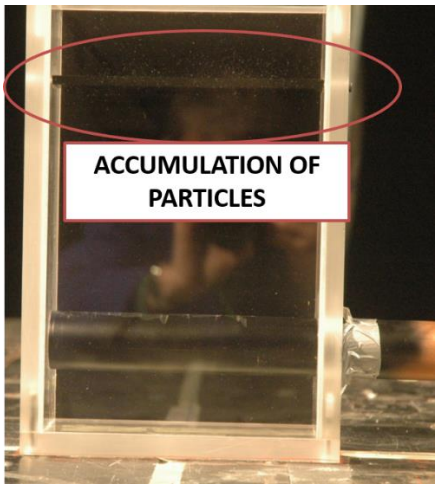


Figure 7. Photograph after introducing the seeding particles for PIV of a filter that is the same as Filter 2 except for the side walls which are now made of methacrylate.

5. Experimental Results and Discussion

Results of the PIV measurements are presented in a three steps discussion process:

Discussion 1: the air intake width is discussed by comparing Filter 1 and Filter 2.

Discussion 2: the mechanical deflector is discussed by comparing Filter 3, Filter 4 and Filter 5

Discussion 3: the effect of the electrostatic force is discussed by comparing the results when the high voltage difference is generated and when there is not this high voltage. Filter 4 has been used for this purpose.

Discussion 1: Effect of the air intake width

The air intake width is discussed by comparing Filter 1 and Filter 2. Figure 8 shows the two average velocity maps corresponding to the Filter 1 and the Filter 2, where the air intake widths are 35 mm and 7 mm respectively and the same pump suction was applied (corresponding to the maximum pump power). As expected, it can be observed in the figure that higher velocities in the air intake, on the order of 27 m/s, are obtained in Filter 2 as compared with those obtained in Filter 1 with the same suction, on the order of 6 m/s. The deflected air velocity is also higher in Filter 2, which means that higher negative horizontal velocity gradients are obtained in the impact wall zone, where particles are collected, as can be observed in figure 9.

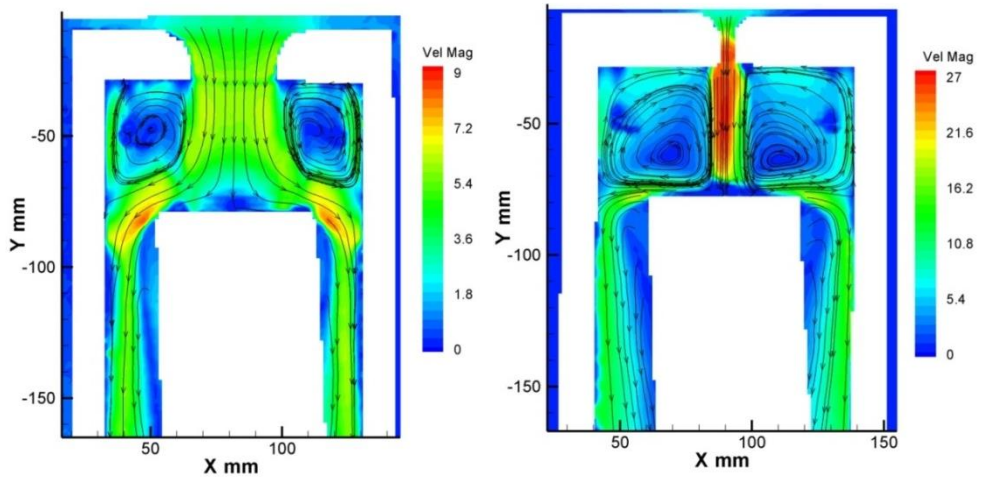


Figure 8. Flow field velocity maps measured by PIV of the Filter 1 (on the left) and Filter 2 (on the right). The magnitude shown is the modulus of the velocity in meter per seconds. Streamlines are superimposed in black to indicate the flow direction.

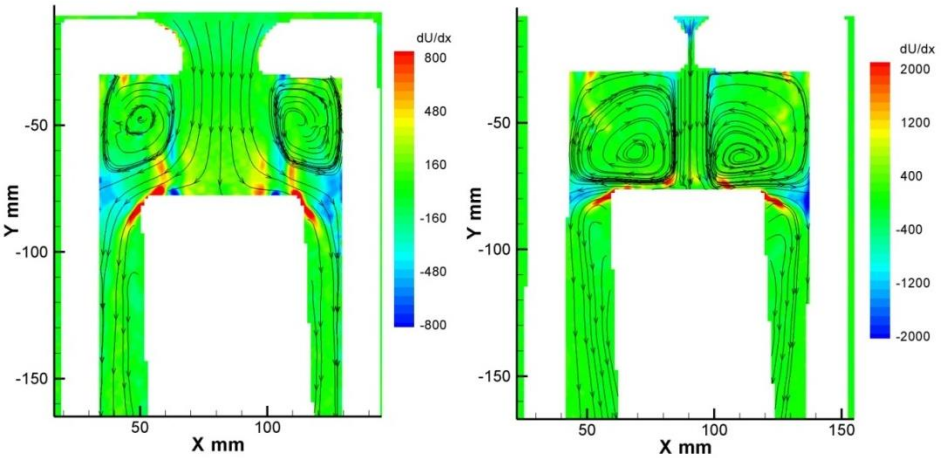


Figure 9. Flow field horizontal velocity gradient maps measured by PIV of the Filter 1 (on the left) and Filter 2 (on the right). The unit of the horizontal velocity gradient is s^{-1}. Streamlines are superimposed in black to indicate the flow direction.

In order to compare the results of Filter 1 and Filter 2 obtained, the velocity flow field inside each filter has been made non-dimensional using the air intake velocity, and the non-dimensional air deflected velocity (which is the ratio between the air deflected velocity and the air intake velocity) has been calculated being higher in Filter 1 (wider air intake) than in Filter 2. Generally, one could think that higher deflected velocity leads to a larger inertia of the particles through the wall, which would increase the number of particles collected and would make the filter more efficient. This means that as long as the flow inside the filters behave in a similar way as shown in Fig. 8 and 9, a wider air intake width for the same total dimensions of the filter and the same air intake velocity would lead to a more efficient filter. However, the air intake velocity obtained in Filter 1 is on the order of 6 m/s, which is small compared to the intake velocity 20 m/s when the filter is under working condition (installed in an aircraft). The flow inside Filter 1 has been simulated numerically for air intake velocities of 6 m/s and 20 m/s in order to ensure that indeed the flow pattern are similar in both cases. The simulation procedure has been the same as explained in section 6. Figure 10 shows the velocity flow field for air intake velocities of 6 m/s (on the left) and 20 m/s on the right. It can be observed that indeed the flow patterns are the same for both cases.

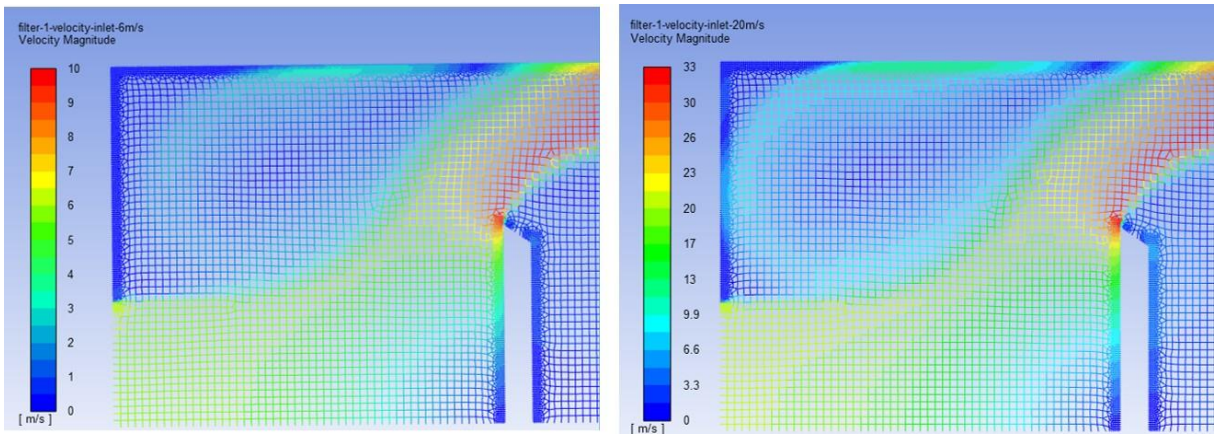


Figure 10. Flow field velocity maps obtained by simulation for the Filter 1 when the air intake velocity was 6 m/s (on the left) and 20 m/s (on the right). The magnitude shown is the modulus of the velocity in meter per seconds.

The pump used during the experiment did not allow to set the air intake velocity at 20 m/s in Filter 1. In order to increase the air intake velocity up to the desired value a more powerful pump would be required or alternatively a smaller filter. On one hand, the increase of the power of the pump is usually associated to an increase in weight, price and it could also pose technical problems related to be embarked on the aircraft. Therefore, there is an upper limit of the power of the pump. On the other hand, a smaller filter leads to smaller caudal, which means that the total amount of particles that pass through the filter decreases and due to the low concentration of bioaerosols in the atmosphere, it could also pose a problem. Therefore, a compromise solution should be chosen regarding the filter size and the pump power.

Discussion 2: Influence of the mechanical deflector

The conceptual approach for the five filters used is the same for all the cases. In an impactor filter the air impinges on a surface where particles, due to its inertia, are collected. The air, that contains the particles, enters the filter in the air intake side (see Figure 3). Then the air encounters a mechanical deflector that throws the air and the particles towards the side walls, where particles are collected. Additionally, a high voltage difference was created between the mechanical deflector electrode and the outer metallic plates acting as sidewalls that pulls the charged particles to the side walls, especially very near the wall retaining the particles in the wall thus increasing the number of particles collected. Therefore, the mechanical deflector is one of the two key features when designing an impactor filter. It could be though as a first approach as a simple flat plate and in this case the deflector width is the most relevant parameter. In an electrostatic filer, as the one studied, it is specially meaningful. The distance between the electrodes (central mechanical deflector and side plates) is directly related to the mechanical deflector width by geometrical consideration only. Therefore, two flat plates of widths of 55 mm and 65 mm are considered for comparison purpose. However, in the electrostatic filter proposed in this investigation, the collection plates are the sides plates and therefore it is interesting to avoid collision in the flat plate. To this end, another mechanical deflector, the one of Filter 5, is tested. Figure 11 shows the three average velocity maps corresponding to the Filter 3, Filter 4 and the Filter 5. Comparing Filter 3 and Filter 4, it can be observed that increasing the width of the flat deflector has little effect on the deflected air velocity. However, modifying the deflector shape influences notably the deflected air velocity. In particular, the mechanical deflector employed in Filter 5 provides higher air deflected velocity and higher negative horizontal velocity gradient in the collector wall zones, as observed in figure 12. Additionally, the main advantage of the Filter 5 as compared to the other filters is that the impact zone observed in the centre of the mechanical deflector has now disappear, and the only impact zone is on the wall, as wanted.

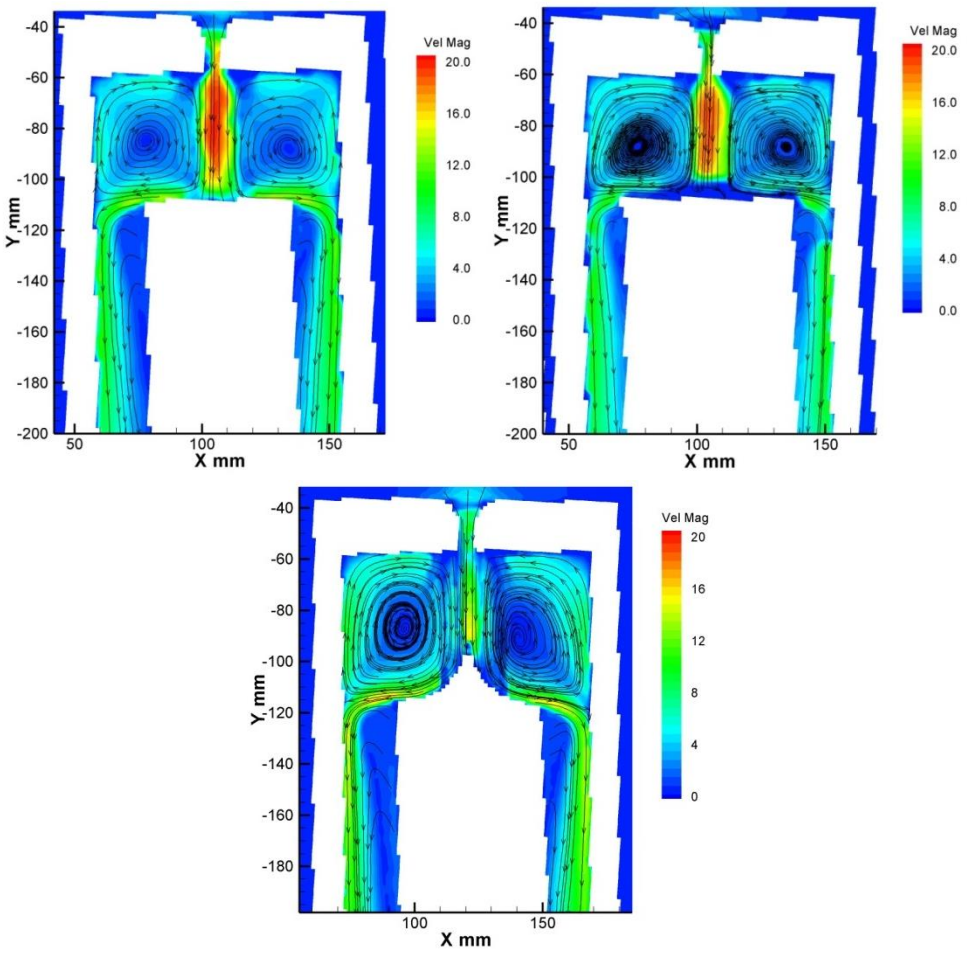


Figure 11. Flow field velocity maps measured by PIV of the Filter 3 (on the top left), Filter 4 (on the top right) and Filter 5 (on the botton). The magnitude shown is the modulus of the velocity in meter per seconds. Streamlines are superimposed in black to indicate the flow direction.

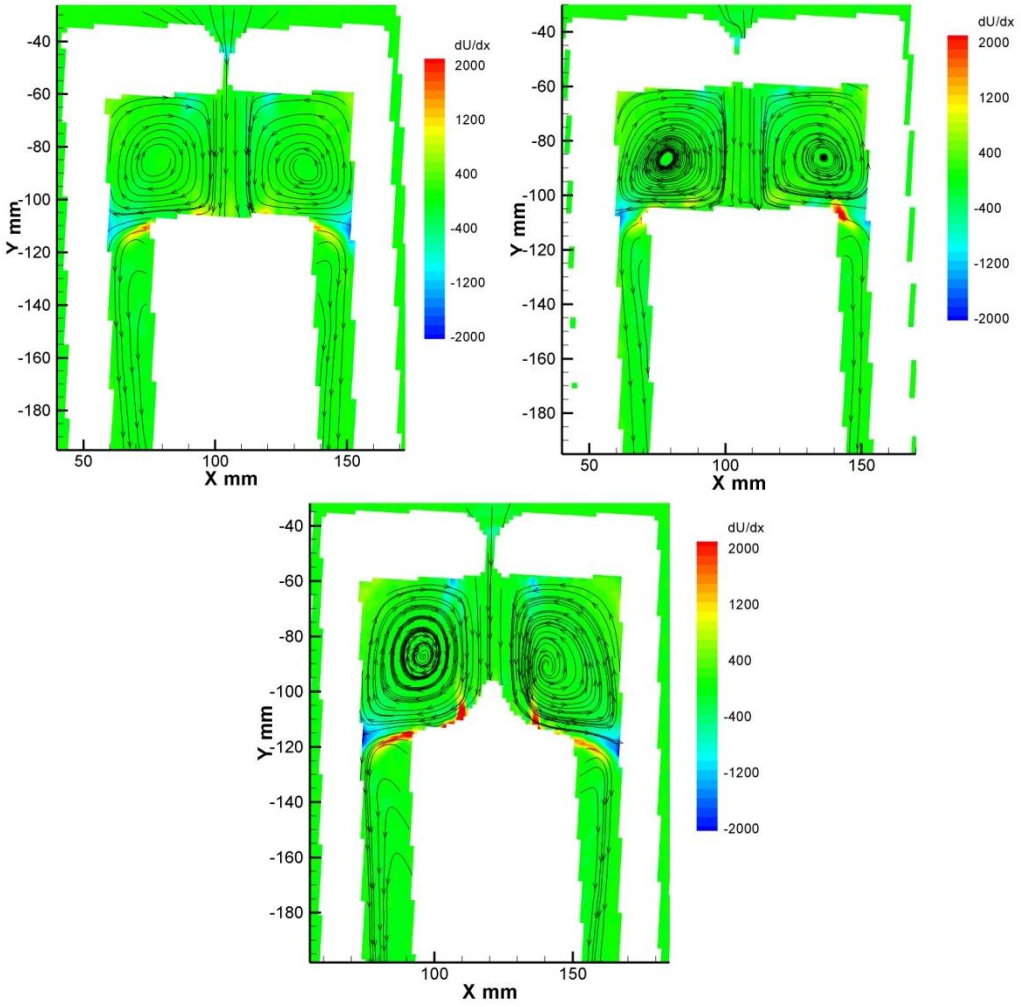


Figure 12. Flow field horizontal velocity gradient maps measured by PIV of the Filter 3 (on the top left), Filter 4 (on the top right) and Filter 5 (on the bottom). The unit of the horizontal velocity gradient is s^{-1}. Streamlines are superimposed in black to indicate the flow direction.

Now, it is interesting to show in more detail the differences found when comparing Filter 3 and Filter 4. The distance between the electrodes in Filter 4 is 22.5 mm, while in Filter 5 is 17.5 mm. A zoom of the differences in velocity gradient in horizontal direction in the wall impact zone is shown in Figure 13. It can be observed that differences are up to 1051 s^{-1}, being greater in absolute value in Filter 4. Since velocities are similar in both cases, this means that Filter 4 has greater deceleration values than Filter 3, being thus more effective to collect particles. In the next section, the influence of the electrostatic force is evaluated in this region.

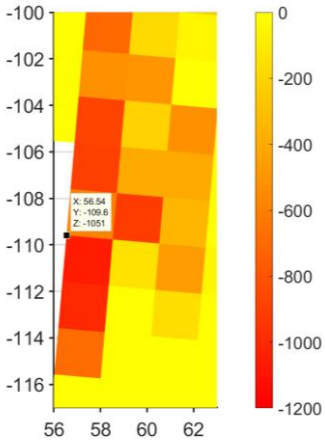


Figure 13. Flow field horizontal velocity gradient map differences between measurement by PIV of the Filter 4 and Filter 3, being positive when values in Filter 4 are greater. The unit of the horizontal velocity gradient is s^{-1}.

Discussion 3: Effect of the electrostatic force

Finally, the effect of the electrostatic force is evaluated. The high voltage generator allow voltages up to 20 KV. Applying 20 KV in filters 3 and 5, no arc discharge was observed, however in filter 4 arc discharges was observed when a voltage of 18.8 KV was applied (see figure 14). This is due to the decrease in the distance between electrodes being in this filter down to 17.5 mm. The deflector edge was also sharped to increase the corona effect.

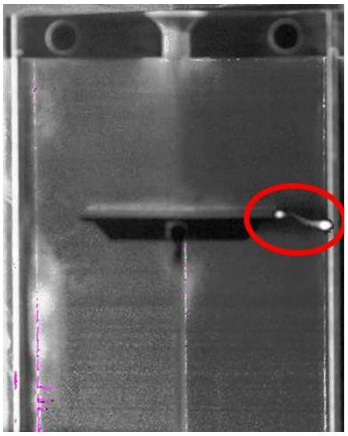


Figure 14. Photograph of the arc discharge observed in Filter 4 when the high voltage applied was 18.8 KV. The arc discharge is marked by a superimposed red oval.

Figure 15 shows the averaged velocity map with and without high voltage applied to the Filter 4. The high voltage applied was 18.6 KV. As observed in figure 15, no meaningful difference is noticed due to the electrostatic force in the flow field inside the filter. However, though the flow field is similar, the electrostatic force acts when the particles are very near the wall helping to retain these particles attached. Moreover, due to the migration velocity generated by the high voltage w_e, the particles would move towards the collecting plate once passed the mechanical deflector, as long as the characteristic time of residence in the filter is larger than the characteristic time to reach the walls.

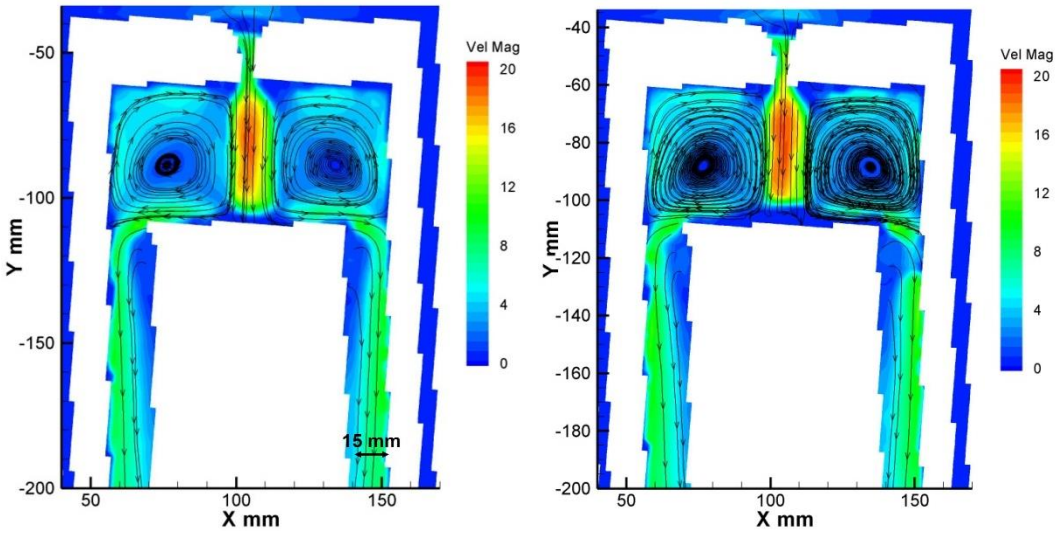


Figure 15. Flow field average velocity maps measured by PIV of Filter 4 with (on the left) and without (on the right) high voltage difference applied. The high voltage applied on the right was 18.6 KV.

Figure 16 shows the nomenclature of a generic filter and the type of flow encountered by experimental tests. The characteristic residence time of the particles once passed the mechanical deflector would be:

$$t_r = \frac{H - h}{v} = \frac{0.25}{12.5} = 0.02\ s$$

The characteristic time to reach the wall due to migration velocity w_e would be calculated as:

$$t_e = \frac{d_e}{w_e}$$

The migration velocity, according to theoretical mathematical models [14] are on the order of 0.3 m/s for particles larger than 2 µm. Therefore, the distance to the wall at which particles would impact the wall and thus be collected due to the high voltage applied would be the following:

$$t_e < t_r \Rightarrow d_e < 6\ mm$$

As seen in Figure 15, this distance ($d_e = 6\ mm$) nearly covers half the distance where the air containing the particles would flow near the walls ($d_w = 15\ mm$). Assuming that the particle concentration at the inlet was homogeneous, the efficiency would the ratio between these two distances (d_e/d_w) and it would be up to 40%. This means that, it would really help the efficiency for particles above 2 µm. The bioaerosol diameter ranges up to 100 µm. For particle less than 2 µm, efficiency tests were carried, and the results are shown in the last section.

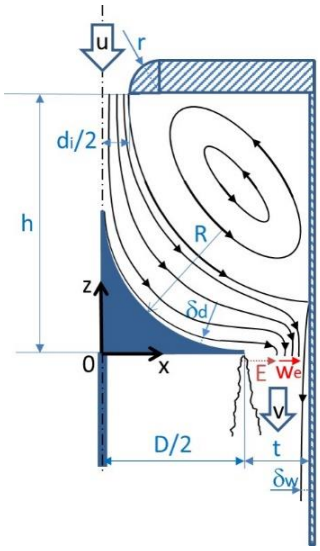


Figure 16. Sketch of a half of the Filter. Nomenclature of the theoretical analysis.

6. Numerical simulations. Stokes Number

The flow field inside the filters has already been studied by PIV experimental test. However, as explained in the section "*Particle Image Velocimetry Validity Discussion*", the results are only valid for particles above 1µm. Therefore, in order to study the Stoke number, computational fluid dynamics (CFD) simulation tests have been conducted using FLUENT for all the five filters under the same inlet conditions. All the five meshes were generated by the Mesh Generator from ANSYS Workbench, limiting the tetrahedral elements size to a maximum of 25K cell mesh, and making refinements close to the walls. Figure 17 shows the mesh of one of the filters.

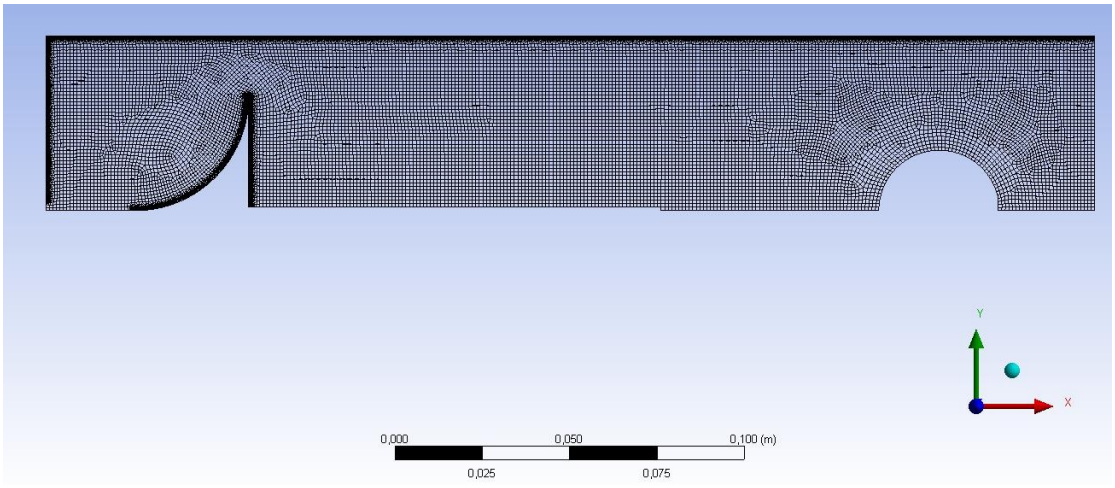


Figure 17. Mesh used for Filter 5.

The velocity maps result with the superimposed streamlines are shown in Figure 18. As can be observed, they are very similar to those obtained by PIV, which validates the simulation conducted.

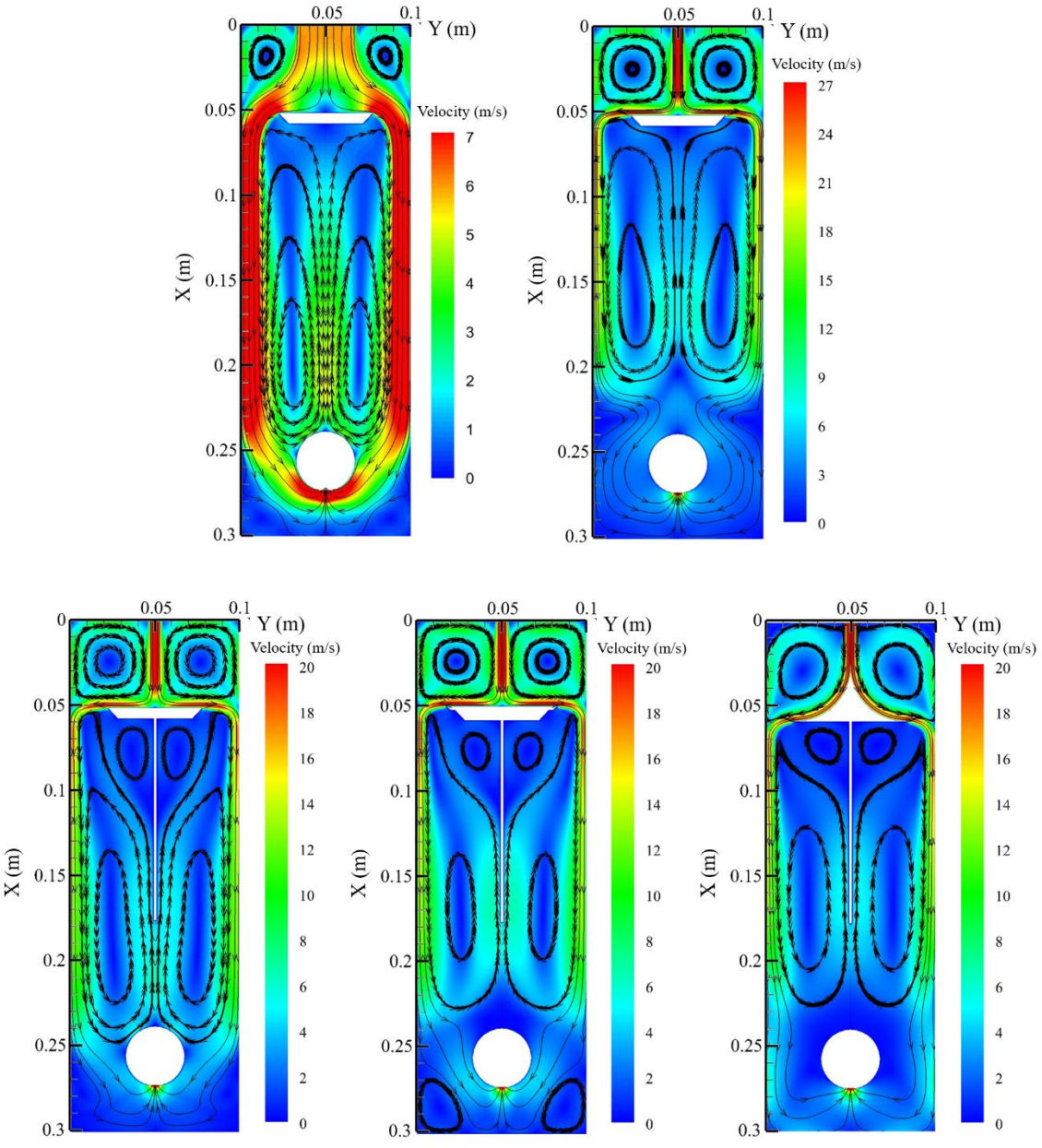


Figure 18. CFD Results of the five filters tested.

For each of the filters, the stagnation line that end in the wall perpendicular and the streamline that contains the maximum velocity due to the mechanical deflector were selected and the Stokes Number and the Reynold Number were calculated based on the lateral velocity and the lateral deceleration found in the simulations. The Stokes Number is defined as the ratio between the characteristic response time τ_s of the particle and the characteristic time of the flow t_c.

$$St = \frac{\tau_s}{t_c}$$

For St <<1, the particles would follow the flow, while for St >1, the particle would not follow the flow, and therefore, it would be filtered by the sampling system. The chacteristic response time of the particle depends on the particle diameter as follows:

$$\tau_s = \frac{d_p^2 \rho_p}{18 \mu_f}$$

On its hand, the characteristic time of the flow generally depends only on the velocity of the flow, the lateral velocity in this case V_y. However, when there are a large decceleration a_c, which is the case, the characteristic flow time could be calculated as follows:

$$t_c = \frac{V_y}{a_c}$$

For each of the filter the characteristic flow time was calculated along the staganation line that ends perpendicular to the wall, and the maximum value was obtained. Using this value the Stokes number is plotted versus the particle diameter in Figure 19. It can be observed that the mechanical deflector that actually reaches Stokes number larger is the one corresponding to Filter 4. It can also be observed that Stokes numbers above the unity are easily found for particles larger 2 µm. Therefore, low efficiencies should be expected for viruses with lower diameter.

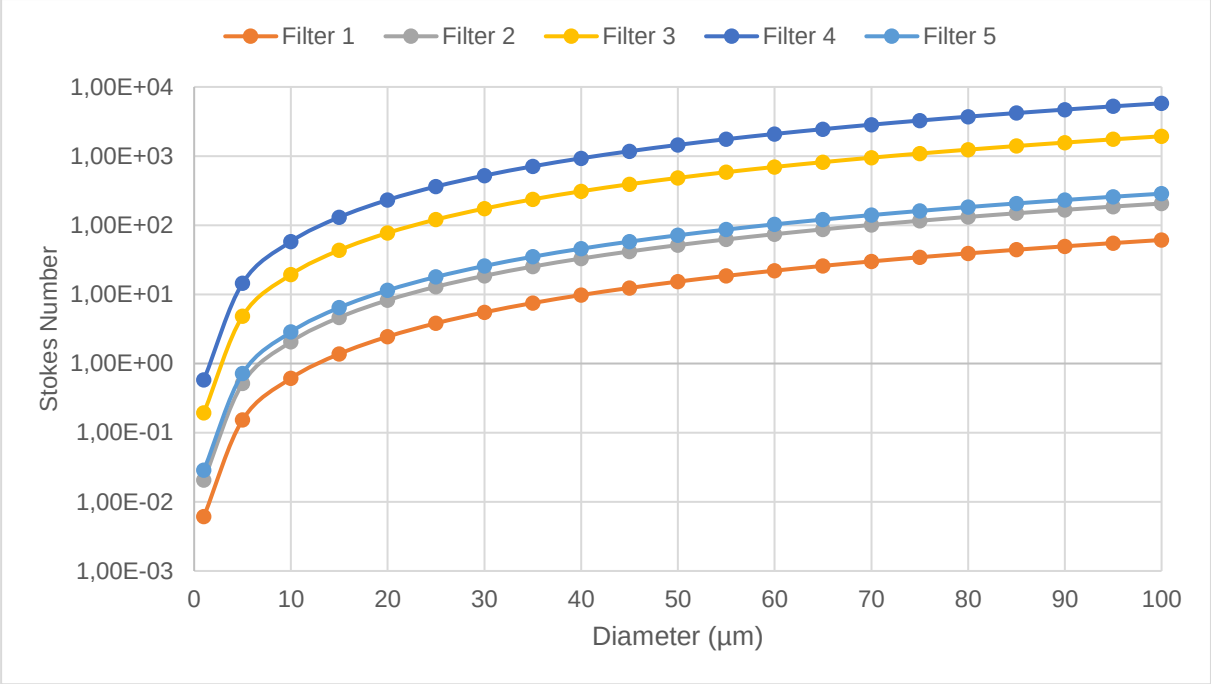


Figure 19. Stokes number versus particle diameter for all the filters tested.

7. Efficiency tests.

Collection efficiency of aerosol samplers are usually defined as the relative recovery in percentage. Table 2 shows the collection efficiency for traditional aerosol sampler for virus-containing aerosols, according to Ref. [15]. It can be observed in the table that the maximum efficiency observed was on the order of 5%. This is a low value, that is in concordance with the simulations conducted in the previous section.

Sampling System	Flow Rate (L/min)	Sampling Time	Other Characteristic	Relative Recovery (%)			
				MS2	Phi X174	T7	Phi 6
Andersen 1STG	28.3	-	24 m/s	1	0.9	0.2-5	0.6
AGI -30	12.5	5 min	-	2	3	0.02-6	0.1
Gelatin Filter	30	5 min	3 µm pore	2	5	0.3-4	0.2
Nucleopore Filter	2	20 min	0.4 µm pore	0.2	0.3	0.003-0.3	0.002

Table 2. Relative Recovery of traditional bioaerosol sampling according to Ref [15].

The efficiency of the Filters 3, 4 and 5 was evaluated experimentally by measuring the relative recovery of an aerosol containing oil particles of diameter of 1 µm, similar to virus diameters. These three filters were chosen because the inlet air velocity was on the order of the real one on-board 20 m/s. The experimental setup for these

efficiency tests can be observed in Fig. 20. A Laskin atomization was used to generate the aerosol, introducing the aerosol generated inside the filter. The final collection efficiency is calculated as the total oil mass m_f recovered divided into the oil introduced in the aerosol in the filter m_{in}. The results are shown in Table 3. The collection efficiency for the new filters are on the order of 8%, which is higher than previous efficiencies.

Sampling System	Filter 3	Filter 4	Filter 5
Collection Efficiency (%)	7.5	7.5	8.5

Table 3. Collection Efficiency of the new prototypes.

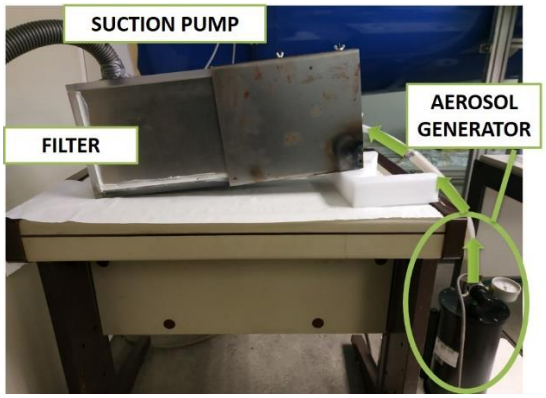


Figure 20. Experimental setup of efficiency tests.

8. Conclusions

The study of microorganism present in the atmosphere by collecting bioaerosols from Investigation Aerial Platforms requires the development of new filters that are specially designed for this purpose. The problems associated to the fact that they are embarked on an aircraft and the low presence of microorganisms need to be addressed. A two-dimensional prototype designed to be embarked in INTA's aerial platforms has been investigated and characterized in order to provide more insight in the physics involved in this type of filters. Five modifications of the filter have been manufactured and tested by means of PIV measurements and numerical simulations, and the velocity maps of flow field inside each modification have been provided. The following conclusions can be stated as follows:

-. If the air intake width is decreased, the ratio of the horizontal velocity in the impact zone in the wall and the intake velocity decreases, which implies that the resultant filter would be less efficient. Therefore, wider air intake widths are preferred.

-. Increasing the plate deflector width poses an advantage, increasing 10% the velocity towards the wall in the wall impact zone when the width has increased 18%. Moreover, the gradual deflector allows greater velocities preventing also the impact of particles in the mechanical deflector.

-. For the configuration studied, the migration velocity originated by the electrostatic forces has turned out to be several magnitude orders less compared to the aerodynamic forces and other effects in the aerodynamic flow have neither been observed. However, the theoretical analysis shows that very near the wall (less than 6 mm), and for bioaerosols larger than 2 µm, the particles would impact the collection plate due to the electrostatic force, thus increasing the efficiency up to 40%.

Numerical simulations have been conducted to study the Stokes number found for each filter showing that higher St numbers are found for Filter 4. Also, Stokes number above the unity are easily found for bioaerosols above 2 µm. For particles on the order of 1 µm, efficiency tests were conducted showing an efficiency on about 8%.

This is a first investigation on filter for bioaerosol flowmetering to be embarked on an aircraft and only a two-dimensional prototype has been investigation. Future studies should comprise axisymmetric configuration that could be based on these results.

Acknowledgements
This research has been partially supported by the Spanish Ministry of Economy and Competiveness (MINECO), under project MICRAS- Scientific missions from manned and unmanned aerial platforms CGL 2015-69758, by the Spanish Ministry of Science, Innovation and Universities under project “Desarollo e implementación de captadores biológicos atmosfericos de altitud: precipitadores electrostáticos de paso unico embarcables en plataformas aereas de investigación” and by the INTA internal project “Termofluidodinámica”.

Nomenclature

a_c	decceleration [m/s^2]
d_e	distance to the side walls [mm]
d_i	intake width [mm]
d_p	particle diameter [mm]
d_w	width of the region where particles are near the sides walls [mm]
h	vertical distance between the deflector and the upper of the filter [m]
t_c	characteristic flow time [s]
t_e	characteristic time to reach the wall [s]
t_r	characteristic residence time [s]
u	intake velocity [m/s]
V_y	lateral velocity [m/s]
w_e	migration velocity [m/s]
μ_f	fluid viscosity
ρ_p	particle density [Kg/m^3]
τ_s	particle characteristic response time [s]
τ_f	characteristic flow time [s]
v	vertical velocity near the side wall [m/s]
D	deflector width [mm]
H	filter height [m]
PIV	Particle Image Velocimetry
St	Stokes number
U	horizontal velocity [m/s]
Vel Mag	velocity magnitude [m/s]
X	horizontal position [mm]
Y	vertical position [mm]

References

[1] Vincent, J. H., Aerosol Sampling: Science, Standards, Instrumentation and Applications. 2007 John Wiley & Sons, Ltd.
[2] Kulkarni, P., Baron, P. A. and Willeke, K., Aerosol Measurement: Principles, Techniques and Applications, 3rd edition. 2011. John Wiley & Sons, Inc. Publications.
[3] Blachere, F. M., Lindsley, W. G., Pearce, T. A., Anderson, S. E., Fisher, M., Khakoo, R., Meade B. J., Landen O., Thewlis, R. E., Celik, I., Chen, B. T., Beezhold, D. H. (2009). Measurement of Airborne Influenza Virus in a Hospital Emergency Department. Clinical Infectious Diseases, 48(4), 438-440.
[4] Dechraksa, J., Suwandecha, T., Maliwan K.and Srichana,T., The Comparison of Fluid Dynamics parameters in an Andersen Cascade Impactor Equipped with and without a Preseparator. American Association of Pharmaceutical Scientists. AAPS Pharm SciTech, Vol. 15, No. 3, June 2014.
[5] King, M. D. and McFarland, A. R. Use of an Andersen Bioaerosol Sampler to Simultaneously Provide Culturable particle and Culturable Organism Size Distributions. Aerosol Science and Technology, 46:852–861, 2012. American Association for Aerosol Research.
[6] Morris, E. J., Darlow, H. M., Peel, J. F. H. and Wright, W. C., The quantitative assay of monodispersed aerosols of bacteria and bacteriophage by electrostatic precipitation. J. Hyg., Camb. (1961), 59, pp. 487-496. Great Britain.
[7] Roux, J. M., Kaspari, O., Heinrich, R., Hanschmann, N., Grunow, R. Investigation of a new electrostatic sampler for concentrating biological and no biological aerosol particles. (2013). Aerosol Science and Technology, 47 (5), pp. 463-471.
[8] Ghosh, B. Lal, H. Srivastava, A. Review of bioaerosols in indoor environment with special reference to sampling, analysis and control mechanisms. (2015). Enviroment International 85 (2015) 254-272.
[9] Haig, C. W., Mackay, W. G., Walker, J. T., Willians, C. Bioaerosol ssampling: sampling mechanisms, bioefficiency and field studies. (2016). Journal of Hospital Infection 93 (2016) 242-255.
[10] Raynor, G. S. Atmospheric Environment. Pergamon Press 1972. Vol. 6, p. 191-196. Great Britain.

[11] Timmons, D. E., Fulton, J. D., Mitchell, R. B., Applied Microbiology, Mar. 1966. American Society for Microbiology. Vol. 14, No. 2.pp. 229-231.
[12] Adrian, R. J. Particle-imaging techniques for experimental fluid mechanics Annual Review of Fluid Mechanics 1991, 23: pp. 261-304.
[13] Prasad, A. K. Particle Image Velocimetry. Current Science, Vol. 79, no. 1, 10, 2000.
[14] Gooch, J. P. and Francis, N. L. A theoretically Based Mathematic Model for Calculationof Electrostatic Precipitator Performance. Journal of the Air Pollution Control Association, 1975, Vol 2, No 2, 108-113.
[15] Tseng, C.C and Li C.-S, Collection efficiencies of aerosol samplers for virus-containing aerosols. Journal of Aerosol Science 36 (2005) 593-607. Elsevier